Petroleum Science 20 (2023) 370–381

Contents lists available at ScienceDirect

Petroleum Science

journal homepage: www.keaipublishing.com/en/journals/petroleum-science

Original Paper

Experimental study of surfactant-enhanced spontaneous imbibition in fractured tight sandstone reservoirs: The effect of fracture distribution

Kun Yang [a, b], Fu-Yong Wang [a, c, *], Jiu-Yu Zhao [a, d]

[a] State Key Laboratory of Petroleum Resources and Prospecting, China University of Petroleum (Beijing), Beijing, 102249, P.R. China
[b] College of Petroleum Engineering, China University of Petroleum (Beijing), Beijing, 102249, P.R. China
[c] College of Artificial Intelligence, China University of Petroleum (Beijing), Beijing, 102249, P.R. China
[d] College of Geosciences, China University of Petroleum (Beijing), Beijing, 102249, P.R. China

ARTICLE INFO

Article history:
Received 27 May 2022
Received in revised form
26 September 2022
Accepted 27 September 2022
Available online 3 October 2022

Edited by Yan-Hua Sun

Keywords:
Tight sandstone
Imbibition
Fracture
Surfactant

ABSTRACT

Spontaneous imbibition is an important phenomenon in tight reservoirs. The existence of a large number of fractures and micro-nano pores is the key factor affecting the spontaneous imbibition of tight reservoirs. In this study, based on high-pressure mercury injection and nuclear magnetic resonance experiments, the pore distribution of tight sandstone is described. The influence of fractures, core porosity and permeability, and surfactants on the spontaneous imbibition of tight sandstone are studied by physical fracturing, interfacial tension test, wettability test and imbibition experiments. The results show that: the pore radius of tight sandstone is concentrated in 0.01–1 μm. Fractures can effectively reduce the oil drop adsorption on the core surface, enhancing the imbibition recovery of the tight sandstone with an increase of about 10%. As the number of fractures increases, the number of oil droplets adsorbed on the core surface decrease and the imbibition rate increases. The imbibition recovery increases with the increase in pore connectivity, while the imbibition rate increases with the increases in core porosity and permeability. The surfactant can improve the core water wettability and reduce the oil–water interfacial tension, reducing the adsorption of oil droplets on the core surface, and improving the core imbibition recovery with an increase of about 15%. In a word, the existence of fractures and surfactants can enhance the pore connectivity of the reservoir, reduce the adsorption of oil droplets on the core surface, and improve the imbibition rate and recovery rate of the tight oil reservoir.

1. Introduction

Tight oil refers to the accumulation of oil stored in tight reservoirs without large-scale migration for a long time. As a kind of unconventional oil and gas, it is known as the “black gold” of the petroleum industry and has broad development prospects (Johnstone, 2007). A large number of micro-nano pores and natural fractures are developed in tight reservoirs, resulting in tight reservoirs have the characteristics of low porosity, low permeability, complex pore-throat structures and strong heterogeneity, which makes it difficult to obtain high oil recovery.

In order to clarify the physical properties and seepage characteristics of tight reservoirs, scholars have done a lot of research on the pore-throat structure and the fluid distribution in the tight reservoir by various methods (Zhang et al., 2019; Lai et al., 2018; Wang et al., 2014; Wang et al., 2018). With the breakthrough of horizontal well technology and volume fracturing technology, the development of unconventional reservoirs such as tight oil has made great progress. A large number of artificial fractures can be generated, and they connect with natural fractures to form a complex fracture network, which greatly improves the fluid flow capacity in tight reservoirs. The large-scale development of tight oil reservoirs has also attracted a lot of attention to the spontaneous imbibition phenomenon (Li et al., 2019; Mason and Morrow, 2013; Meng et al., 2017).

Spontaneous imbibition refers to the process in which the wetting phase spontaneously enters the core pores to displace the non-wetting phase under the action of capillary force. The most common imbibition methods in the laboratory include imbibition

* Corresponding author. State Key Laboratory of Petroleum Resources and Prospecting, China University of Petroleum (Beijing), Beijing, 102249, P.R. China.
E-mail address: wangfuyong@cup.edu.cn (F.-Y. Wang).

https://doi.org/10.1016/j.petsci.2022.09.033

cells, and the weighing method (Wang et al., 2017; Zhou et al., 2016). With the maturity of nuclear magnetic resonance (NMR) technology and CT technology, they are also widely used to monitor the fluid distribution during imbibition (Cheng et al., 2019; Dai et al., 2019; Liu et al., 2020; Schembre and Kovscek, 2001; Shi et al., 2011). Influence factors of imbibition are always the focus of research. A large number of imbibition experiments and theoretical studies have shown that spontaneous imbibition is affected by various factors (Deng and King, 2019; Ning et al., 2022; Saputra et al., 2019; Zhang et al., 2018; Wang and Zhao, 2021a; Wang and Zhao, 2021b), such as rock physical properties, oil–water properties, and boundary conditions. Alvarez et al. (2018) studied the adsorption phenomenon of surfactant on the surface of shale, and analyzed the effect of surfactant adsorption on imbibition. Xu et al. (2019) used different surfactants to study the effects of interfacial tension and wettability on the imbibition law of low-permeability reservoirs and observed that changing wettability and reducing interfacial tension can effectively improve the recovery of low-permeability reservoirs. Guo et al. (2020) conducted imbibition experiments using tight sandstones in the Ordos Basin and discussed the effects of permeability, salinity, interfacial tension, and other factors on imbibition recovery and imbibition stabilization time. Cai et al. (2020) found that the presence of wetting clay minerals in tight sandstone can enhance the core imbibition capacity. Yu et al. (2021) studied the spontaneous imbibition mechanism of oil–water surfactants through fracture–matrix microfluidic chips of different sizes. Zhang et al. (2022) studied the mechanism of nanofluids to enhance imbibition recovery.

Natural fractures in tight reservoirs and the complex fracture network formed in the development process make the influence of fractures on tight reservoir imbibition cannot be ignored. Xie et al. (2018) studied the dynamic imbibition phenomenon of low permeability reservoir under high temperature using artificial cores. They found that the flow of fluid in micro-fractures has a significant impact on the imbibition rate of low permeability cores, and improving the water wettability can significantly improve the seepage capacity between core matrix and fracture. Gao et al. (2018) studied the imbibition mechanism of fractured tight cores by the weighing method. Research shows that fractures can effectively improve the core imbibition recovery, and the core imbibition rate decreases with the increase in core length. The research of Yang et al. (2019) shows that the imbibition rate and recovery are closely related to the core permeability. Fractures can increase the imbibition contact area and imbibition scope, thereby improving the imbibition rate and recovery.

Fractures play a very important role in enhancing oil recovery in tight oil reservoirs. Scholars have done a lot of research on the influencing factors of imbibition, but there still is a lack of experimental research on the effect of fractures on imbibition. At the same time, scholars pay little attention to the change of imbibition rate and the adsorption process of oil droplets on the core surface during imbibition process. In order to clarify the effect of fractures on the imbibition of tight reservoirs, physical fracturing, high-pressure mercury injection, nuclear magnetic resonance, interfacial tension test, wettability test and imbibition experiments were carried out. The effects of fractures on tight sandstone recovery and imbibition rate were studied. The distribution of oil droplets on the core surface during the imbibition process was observed and the influence of fractures on the imbibition process of tight sandstone was analyzed. At the same time, the factors affecting imbibition such as core porosity and permeability characteristics, interfacial tension, and wettability were studied.

2. Geological setting

Ordos Basin, located in the midwestern China, with a total area of about 37×10^4 km^2, is the second largest petroliferous sedimentary basin in China. The structure of the Ordos Basin rises in the east and descends in the west, with a slope of less than 1° per kilometer. Ordos Basin has experienced the whole process of formation, development, expansion, contraction and even extinction of lake basin (Li et al., 2022). With the evolution of the lake basin, several major provenance areas at the boundary of the basin provided sufficient sedimentary clastic components, forming a lacustrine delta clastic reservoir with large sedimentary thickness (Song, 2021).

The Upper Triassic Yanchang Formation is the main oil-bearing formation in the Ordos Basin. On the whole, the total thickness of the stratum is 1000 m, the main rock is yellow-green and gray-green sand mudstone, and the main sedimentary facies is lake-delta facies. According to the analysis of lithology, cyclic depositional law and tectonic evolution, the Yanchang Formation is divided into 10 oil layer groups from top to bottom. Among them, the Chang 7 oil layer group, as the source rock layer deposited in the heyday of lake basin development, has the characteristics of self-generation and self-reservoir. The main mineral components of sandstone in Chang 7 layer are quartz, feldspar, and detritus. The main distribution interval of porosity is 8%–12%, and the permeability is $(0.05–2) \times 10^{-3}$ μm^2. According to the classification standard of reservoir physical properties, this layer belongs to low porosity and ultra-low permeability reservoir (Liu, 2018).

In recent years, with the development of science and technology, unconventional oil and gas resources have been developed on a large scale, and the Chang 7 oil reservoir group is one of the key targets for exploration and development. Scholars have also conducted a lot of research on the reservoir properties and seepage laws of the Chang 7 oil layer group in the Ordos Basin.

3. Experiments

3.1. Experimental materials

In this study, a total of 16 tight sandstone samples from the Chang 7 Formation in the Ordos Basin were selected for the experiments. The tight sandstone cores have a length of 5.010–5.732 cm and a diameter of about 2.5 cm, the permeability varies from 0.013 to 0.195 mD and porosity is between 3.414% and 12.081%. The core parameters are shown in Table 1.

The oil used in the experiment is the simulated oil, which is made of crude oil and kerosene in a ratio of 1:1. The density of the simulated oil is 0.798 g/cm^3 and the viscosity is 4.8 mPa·s at 35 °C and 101.3 kPa. The salinity of formation water used in the experiment is 20000 mg/L. The surfactant imbibition solution used in the experiment was dodecylbenzene sulfonate solution (SDBS), and the mass concentrations were 0.05%, 0.15%, and 0.20%, respectively. The properties of SDBS used are shown in the Table 2.

3.2. Experimental method

3.2.1. High-pressure mercury injection (HPMI) experiment

High-pressure mercury injection (HPMI) is a process in which the non-wetting phase is used to displace the wetting phase, based on the capillary bundle model. By continuously changing the injection pressure, the mercury injection volume under different injection pressures can be obtained, thereby obtaining the capillary

Table 1
Parameters of experiment cores.

Core No.	Length L, cm	Diameter d, cm	Porosity ϕ, %	Permeability K, mD	Experimental method
1	5.690	2.490	11.398	0.041	Imbibition, NMR
13	5.536	2.470	11.918	0.033	Imbibition, NMR
20	5.010	2.474	12.081	0.195	Imbibition, NMR
2	5.678	2.500	8.933	0.018	Imbibition
3	5.622	2.516	7.441	0.018	Imbibition
4	5.600	2.512	11.450	0.036	Imbibition
8	5.530	2.482	2.973	0.004	Imbibition
10	5.732	2.502	3.414	0.030	Imbibition
14	5.716	2.492	7.544	0.013	Imbibition
19	5.680	2.500	7.228	0.028	Imbibition
5	4.694	2.522	12.110	0.105	Fracturing, Imbibition
11	5.677	2.493	7.930	0.073	Fracturing, Imbibition
16	5.616	2.495	9.020	0.086	Fracturing, Imbibition
8A	2.497	2.494	13.51	0.189	HPMI
18A	2.483	2.518	8.92	0.063	HPMI
24A	2.488	2.518	11.97	0.011	HPMI

Table 2
Surfactant descriptions.

Surfactant	Type	HLB	pH	Purity	Manufacturer
SDBS	Anionic	10.638	7	>97%	Tianjin Xiangruixin Chemical Technology Co., Ltd.

force curve. HPMI can measure many parameters, such as the maximum pore radius, median pore radius, sorting coefficient, and skewness, and quantitatively characterize the pore-throat structure of the core.

In this study, three tight sandstones (Wang et al., 2019) were selected for this experiment, and the core parameters are shown in Table 1. After the core was cleaned and dried, it was tested by the American AutoPore IV 9505 mercury porosimeter. The maximum mercury injection pressure in the experiment is 80 MPa. Under this pressure, the mercury saturation values of the cores are over 90%.

3.2.2. Nuclear magnetic resonance (NMR) experiment

Nuclear magnetic resonance (NMR) can obtain the pore and fluid distribution by measuring the relaxation characteristics of the fluid in the core pores, without damaging the core. Nuclear magnetic resonance instrument Oxford was performed at 35 °C. The echo interval of 0.3 ms was used in the experiment, and 64 scans of the core were performed, and 2048 echoes were obtained. In this study, the NMR curves of the three cores in different saturated media were measured respectively.

3.2.3. Physical fracturing

Three cores were selected for physical fracturing experiments. Core permeability was measured before and after fracturing.

3.2.4. Interfacial tension test and wettability test

The main action mechanisms of surfactants include reducing interfacial tension and changing wettability. In order to study the effect of surfactant on imbibition recovery, the oil–water interfacial tension and core surface wettability were tested.

In this study, the interfacial tension meter SVT20 was used to measure the interfacial tension between oil and different imbibition fluids. The centrifugal speed of the experiment was 6000 r/min. The oil droplets will stretch and deform a certain curvature under the action of high centrifugal force that can be captured by a high-precision camera to calculate the oil–water interfacial tension.

The contact angle between the oil droplet and the core was measured. The core pieces were cleaned and dried, and then soaked in imbibition fluid for 48 h. At 35 °C and 101.3 kPa, the contact angle between oil droplets and the core surface in the imbibition fluid was measured with a high-magnification microscope.

3.2.5. Imbibition experiment

The low porosity of tight sandstone results in less saturated oil volume in the core. To ensure the experimental accuracy of the volume method, the imbibition cells with an accuracy of 0.01 mL are selected for the imbibition experiment, as shown in Fig. 1. The procedures of the imbibition experiment are as follows:

1) Dry the cores and then vacuum for 12 h. Saturate cores at 25 MPa for 12 h. After saturation, place them in simulated oil for 12 h to make them fully saturated.

Fig. 1. Imbibition cell with the accuracy of 0.01 mL.

2) Take out the cores from the simulated oil and remove the oil slick on the core surface. Then put the cores into the imbibition cells.
3) Add the imbibition liquid to submerge the cores, ensuring the imbibition liquid enters the appropriate position. Seal the imbibition cells and put them into a 35 °C incubator.
4) Record the volume of oil produced at different times from the time that the solution contacts the bottom of the cores, and take photos to record the changes of oil droplets on the core surface simultaneously.

4. Results

4.1. Capillary pressure curves and pore distribution measured by HPMI

The capillary force curves and pore distribution curves of three cores are shown in Fig. 2. The core permeability obtained from the high-pressure mercury injection experiment is 0.011–0.189 mD, and the porosity is 8.92%–13.51%. It can be found that there are certain differences in the capillary force curves of different cores, indicating that there are certain differences in the pore structure inside the cores. The displacement pressure of Core 8A is relatively small, and there are more large pores in this core. Core 24A has a higher displacement pressure, an upward capillary force curve, which indicated a smaller pore radius. According to the core capillary force curve, the pore distribution curves of cores can be obtained, as shown in Fig. 2b. The pore distribution of Core 8A ranges from 0.009 to 2.806 μm, and the pore distribution is the most extensive. The pore radius of Core 24A ranges from 0.009 to 0.540 μm, concentrated at about 0.1 μm. Core 18A has a pore distribution ranging from 0.009 to 0.771 μm. It can be found from Fig. 2a that when the mercury saturation is greater than 50%, the capillary force of Core 18A rises rapidly, and the pore distribution curve of the core has obvious double peaks. The larger pores are concentrated in 0.1–0.2 μm, and the smaller pores are concentrated in 0.009–0.02 μm. At the same time, it can be found that with the increase of core permeability, the maximum pore radius and average pore radius increase, and the core pore distribution curves move to the right.

The pore throat parameters of cores are shown in Table 3. The core sorting coefficient obtained by HPMI is between 1.945 and 2.72. With the increase in the core sorting coefficient, the core pore distribution range becomes larger. The skewness of the cores is greater than 0, which means the core homogeneity is strong, and relatively coarse pores account for more.

The pore distribution curve measured by the HPMI method depends on the mercury injection pressure. The limitation of the injection pressure makes it impossible to accurately measure the small pore volume in the cores. At the same time, due to the influence of the capillary end effect, the influence of the displacement pressure needs to be considered, resulting in the distribution of large pores calculated by HPMI having certain errors.

4.2. Core pore measured by NMR

Three cores were selected for the NMR experiment. The permeability of the three cores is 0.033, 0.041, and 0.195 mD, respectively, and the porosity is similar, ranging from 11.398% to 12.081%. The NMR spectra of the three cores in different saturated media are shown in Fig. 3.

From the NMR spectra, it can be found that the T_2 distribution curve under oil-saturated conditions is skewed to the right, which may be due to the stronger H signal of oil. At the same time, the cumulative pore distribution curve under oil-saturated conditions is slightly lower than that under water-saturated conditions, which may be because the oil viscosity is higher, and it cannot enter smaller pores when the cores was saturated at the same pressure.

Studies have shown that the NMR relaxation time has a power exponential relationship with the core pore radius (Li et al., 2015; Volokitin et al., 2001):

$$r = C \cdot T_2^{1/n}$$

where T_2 is the transverse relaxation time, ms; r is the pore radius, μm; C and n are constants.

Liu (2019) studied the conversion relationship between NMR relaxation time and radius of Chang 7 cores in the Ordos Basin, and obtained the conversion coefficient of NMR relaxation time and radius. They got the conversion coefficient $C = 0.09$ and $n = 0.725$, which are adopted in this paper to calculate the pore radius.

The pore distribution curves after conversion are shown in Fig. 4. The pore radius is concentrated in 0.01–10 μm. Comparing the pore distribution curve converted from the T_2 spectrum with the pore distribution curve obtained by HPMI, it is found that there are significant differences in the pore distribution range between them. The pore distribution range obtained by the T_2 spectrum is more extensive, and the distribution of pores with a pore radius of

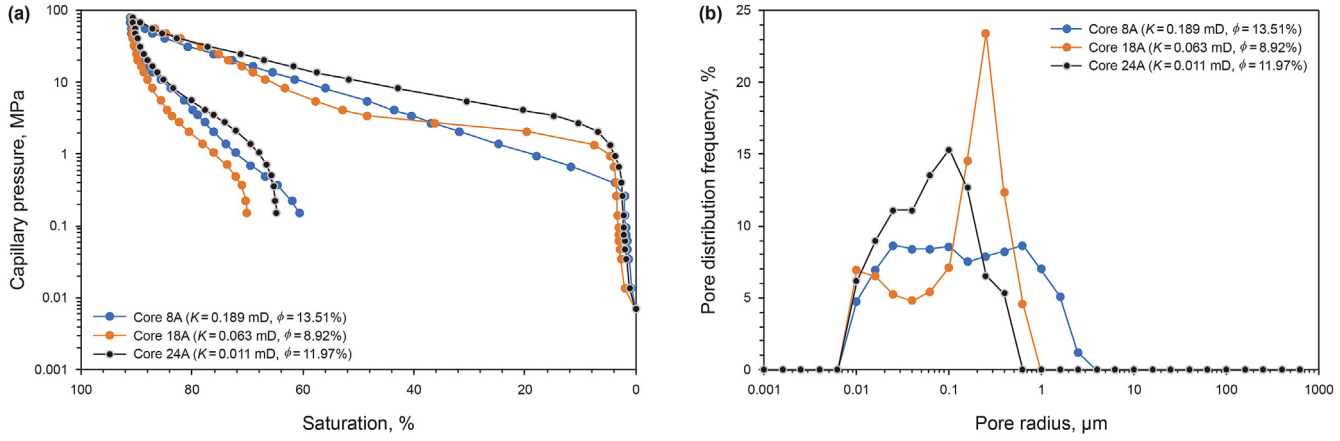

Fig. 2. Capillary pressure curves and pore distribution curves obtained by HPMI.

Table 3
Core parameters measured by HPMI experiment.

Core No.	Porosity, %	Permeability, mD	Maximum pore radius, μm	Mean pore radius, μm	Media pore radius, μm	Sorting coefficient	Skewness	Displacement pressure, MPa	Efficiency of mercury withdrawal, %
8A	13.51	0.189	2.806	0.497	0.129	2.72	0.064	0.262	33.466
18A	8.92	0.063	0.771	0.222	0.19	2.28	0.524	0.953	22.857
24A	11.97	0.011	0.540	0.119	0.072	1.95	0.194	1.360	28.661

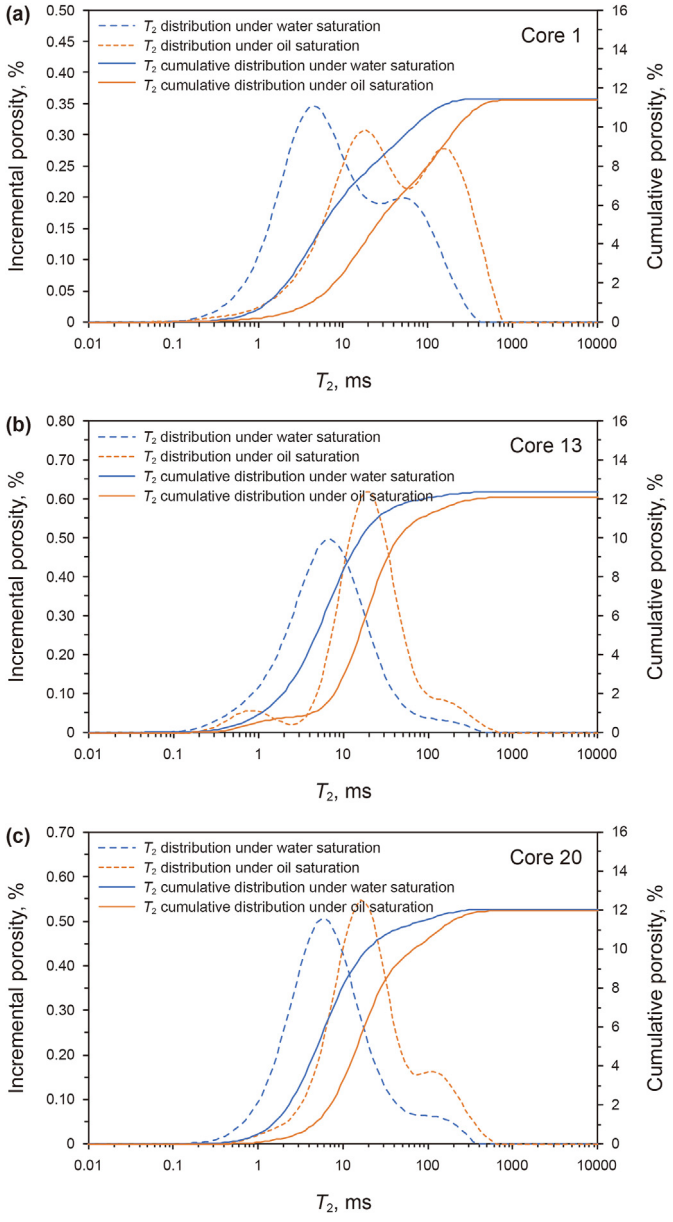

Fig. 3. NMR spectra of 3 cores under oil-saturated conditions and NMR spectra of 3 cores under water-saturated conditions.

0.001–0.01 μm and greater than 10 μm can be seen intuitively. The proportion of pores with a pore radius between 0.001 and 0.01 μm is small, about 4%–8%, and the proportion of pores larger than 10 μm is about 1%–3%.

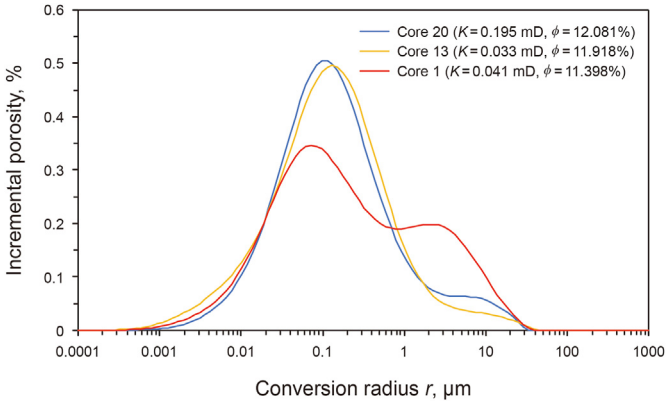

Fig. 4. Pore distribution curves after conversion based on NMR experiment.

4.3. Core properties after fracturing

The cores after fracturing are shown in Fig. 5, the fractures are masked by red lines. Due to the different texture structures of the cores, some horizontal fractures generated in the fracturing process. According to the different distribution of core fractures, the cores after fracturing is divided into single fracture cores and cross fracture cores. The parameters of each core before and after fracturing are shown in Table 4. Before fracturing, the core porosity ranges from 7.979% to 13.641%, and the permeability ranges from 0.086 to 0.105 mD. After fracturing, the core permeability increases significantly, and the permeability of Core 5 increases by about 258 times.

When the core confining pressure increases, the fracture aperture will decrease. In this study, the liquid permeability of the core under different confining pressures is measured to judge the influence of confining pressure on the core.

The liquid permeability of each core under different confining pressures are shown in Fig. 6. It can be found that the core liquid permeability decreases with the increase in confining pressure, and they are in a linear relationship in the semi-logarithmic diagram. According to Darcy's law, the core permeability is directly proportional to the core fracture aperture. The greater the core permeability, the greater the fracture aperture. Therefore, it can be inferred that the core confining pressure is inversely proportional to the fracture aperture, and the fracture aperture decreases with the increase in confining pressure.

4.4. Interfacial tension and wettability

The measured interfacial tension is shown in Table 5. It can be seen that the interfacial tension between distilled water and oil is the largest, followed by the formation water. As the concentration of surfactant increases, the oil–water interfacial tension decreases.

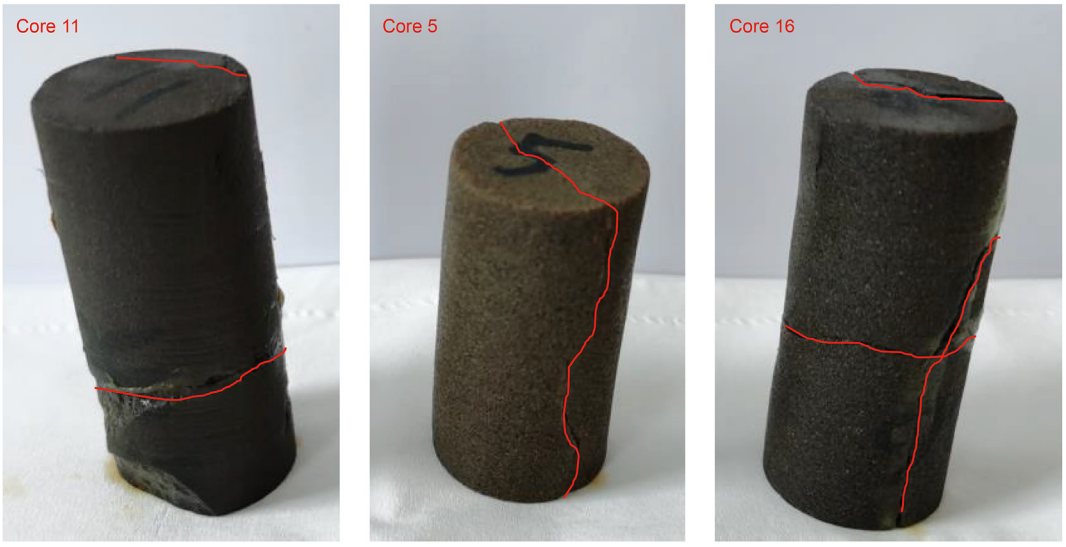

Fig. 5. Oil-saturated cores after fracturing.

Table 4
Core parameters before and after fracturing.

Core No.	Length, cm	Diameter, cm	Initial Permeability, mD	Permeability after fracturing, mD	Increasing times of permeability	Fracture aperture, μm	Type of fracture
5	4.694	2.522	0.105	27.209	258.133	1.64	Single fracture
11	5.677	2.493	0.073	0.136	0.874	0.09	Cross fracture
16	5.616	2.495	0.086	15.478	178.979	1.43	Cross fracture

A summary of the contact angles of each core in different imbibition fluids is shown in Table 6. Some core contact angles measured are shown in Fig. 7. It can be found that the contact angle between the oil droplet and the core slice in the formation water is between 44° and 67°, indicating that experimental cores are water-wet. After adding the surfactant, the contact angle decreased slightly, ranging from 41.34° to 50.47°, indicating the water wettability of the core increased slightly.

4.5. Imbibition results

The imbibition results of 13 tight sandstones are shown in Table 7. The saturation of tight sandstone is more than 78% at 25 MPa. The saturation of Core 10 and Core 11 is greater than 1, which may be due to the high saturation pressure, resulting in micro-fractures in the tight sandstone. In addition, due to small core porosity, the existence of systematic error in the weighing process may also make their saturation greater than 1. The recovery at different times in the imbibition process is shown in Fig. 8. It can be found that there are certain differences in the imbibition recovery rate of different cores. The difference in the core imbibition recovery is caused by many factors. Based on the experimental results, the influences of fracture, core porosity and permeability, and surfactant on imbibition are discussed in the next section.

5. Discussion

5.1. Effect of fracture on imbibition

The imbibition recovery and imbibition rate of 3 fractured cores and 2 control cores are shown in Fig. 9. It can be seen that the core imbibition recovery shows a significant increase after the physical fracturing, with a maximum increase of about 10% (Core 11). Comparing the imbibition rate of each core, it can also be found that the core imbibition rate shows a certain increase after fracturing. Core 5 has a single fracture and Core 11 has a cross fracture. When the imbibition liquid is formation water, compared with Core 20, the maximum imbibition rate of Core 5 increases by about 5 times, and the maximum imbibition rate of Core 16 increases by more than 10 times. This indicates that the existence of fractures can increase the imbibition rate of the tight sandstone, and with the increase in the number of fractures, the imbibition rate increases. After the core imbibition rate reaches the maximum value, the imbibition rate begins to decrease. As shown in Fig. 9, Core 16 imbibition rate decreases the fastest, followed by Core 5, and Core 20 is the slowest, indicating that there is a certain correlation between the core imbibition decline and the core imbibition growth. The faster the core imbibition rate increases, the faster it decreases accordingly. Therefore, large-scale fracturing can improve the initial production rate of the oilfield, but the production rate decreases rapidly in the later stage of oilfield production. Fracturing should be carried out reasonably in the actual development process.

At the same time, it can be found from Fig. 9 that when the imbibition liquid is the same, the time when oil starts to be produced from fractured tight sandstone is earlier than that of the unfractured core. This indicates that the existence of fractures not only increases the contact area between the core and the imbibition fluid, enhances the imbibition effect of the pores, but also provides a seepage channel for the fluid flow, which accelerates the fluid production rate in the core.

In this study, the oil droplets on the core surface during the imbibition process were observed, as shown in Fig. 10. It can be seen that at the beginning of imbibition, oil droplets first appeared at the fractures of the core, and with the increase in time, the oil droplets gradually became larger and eventually separated from

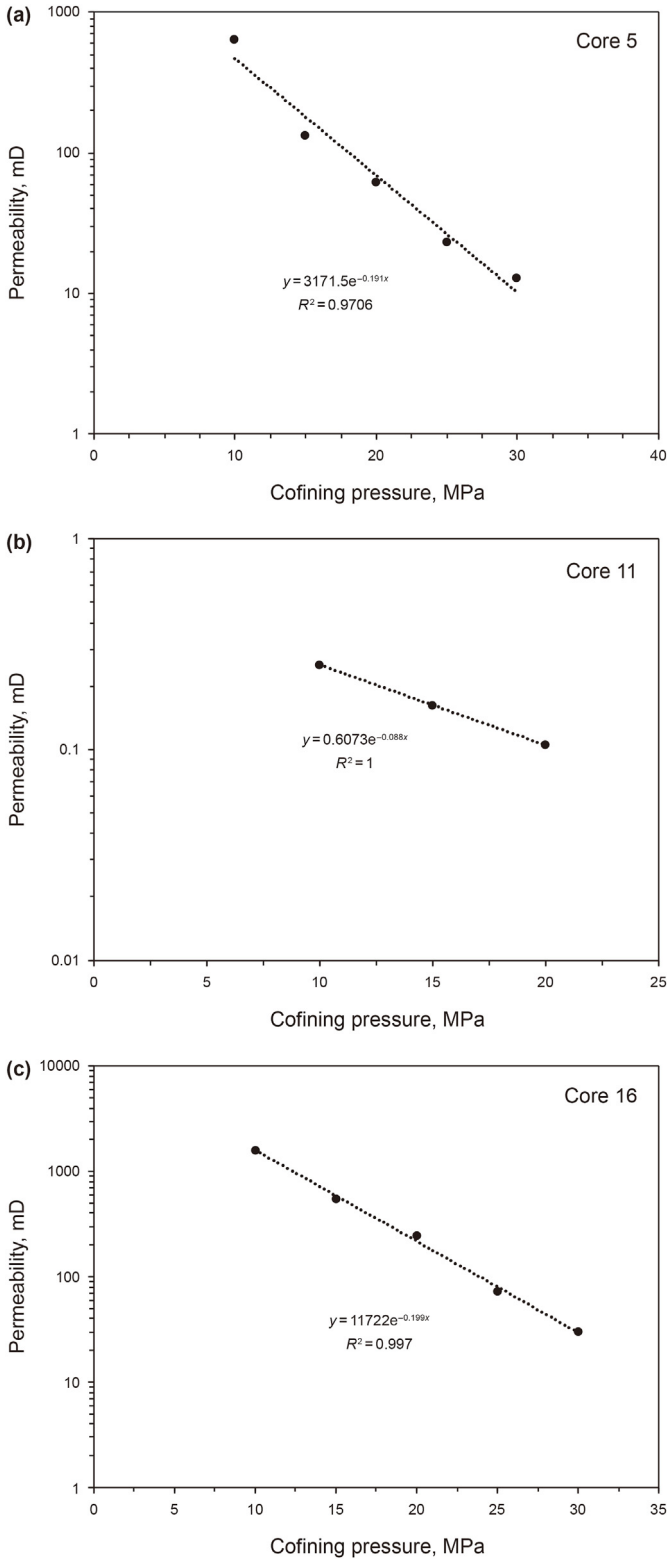

Fig. 6. Core permeability under different confining pressures.

the core surface. Though imbibition fluids of Core 5 and Core 16 both are formation water, the distribution of their oil droplets on the core surface is different. The number of oil droplets adsorbed on the surface of Core 16 is relatively less. This is because that the fracture distribution of Core 5 and Core 16 is different. The cross fractures of Core 16 make the number of fractures more than Core 5. During the core imbibition process, the oil produced by matrix imbibition is mainly discharged through the fractures, resulting in few oil droplets adsorbed on the core surface with the increase in fractures.

In addition, it can be found from Fig. 10 that the radius of the oil droplets adsorbed on Core 5 is relatively large. This is because that the interfacial tension between the formation water and the simulated oil is large, and the small oil droplets cannot be separated from the core surface in time. The oil droplets at the core surface continue to accumulate, forming large oil droplets. While the oil droplets in Core 16 are mainly produced at the fractures, and more fractures in the core make the oil droplets in the core easier to flow, which is also the main reason why the imbibition rate of the Core 16 is relatively large at the beginning of the imbibition.

5.2. Effect of porosity and permeability on imbibition

The imbibition fluid in this study is dodecylbenzene sulfonate (SDBS) with a mass concentration of 0.15%. Comparing the recovery with core porosity and permeability, it is found that there is no obvious correlation. For example, the porosity and permeability of Cores 8, 2, and 4 increase in turn, but the imbibition recovery of these cores do not change significantly. At the same time, comparing Cores 4 and 13, it can be found that although their porosity and permeability are similar, the difference in imbibition recovery between them is nearly 10%. The results show that only the porosity and permeability of the core cannot directly characterize the core imbibition capacity. It can be found from Table 7 that the oil saturation of these cores are different, which reflects the pore connectivity in the cores to a certain extent. Except that Core 10 has a large error due to the excessively low porosity, it has a certain relationship between the core imbibition recovery and the core saturation. The reason that the imbibition recovery of Cores 13 and 19 is significantly higher than other cores may be due to the better connectivity. Liu et al. (2021) also discussed the effect of pore connectivity on spontaneous imbibition in their study. They found that the mainstream imbibition area of the core increase with the pore connectivity and can be regarded as a good indicator of the imbibition efficiency of tight sandstone.

However, comparing the imbibition rate with core porosity and permeability, it can be found that with the core porosity and permeability increase, the imbibition rate increase in the initial stage of imbibition, and the imbibition rate decays rapidly in the middle and late stages of imbibition. As shown in Fig. 11, Core 4 has the largest porosity and permeability, its imbibition rate is much higher than that of other cores at the initial stage of imbibition. With the progress of imbibition, the core imbibition rate decreases rapidly, which is lower than other cores with similar permeability.

In addition, it can be found from Fig. 11 that the imbibition rate of Cores 8 and 10 is much lower than that of other cores, and the time the oil starts to be produced is later than others. Even after the

Table 5
Interfacial tension between oil and different imbibition fluids.

Imbibition fluid type	Distilled water	Formation water	0.05% SDBS	0.15% SDBS	0.20% SDBS
IFT, mN/m	14.91	10.62	7.23	4.67	3.63

Table 6
Contact angles between oil droplets and cores in different imbibition fluids.

Core No.	Contact angles of formation water, °	SDBS	
		Mass concentration, %	Contact angles, °
1	64.08		
2	46.38	0.15	42.47
3	49.41	0.05	46.69
4	55.39	0.15	50.47
8	54.59	0.15	49.70
10	56.95	0.15	45.05
13	44.45	0.15	43.06
14	51.58	0.20	47.75
19	48.72	0.15	41.34
20	66.87		

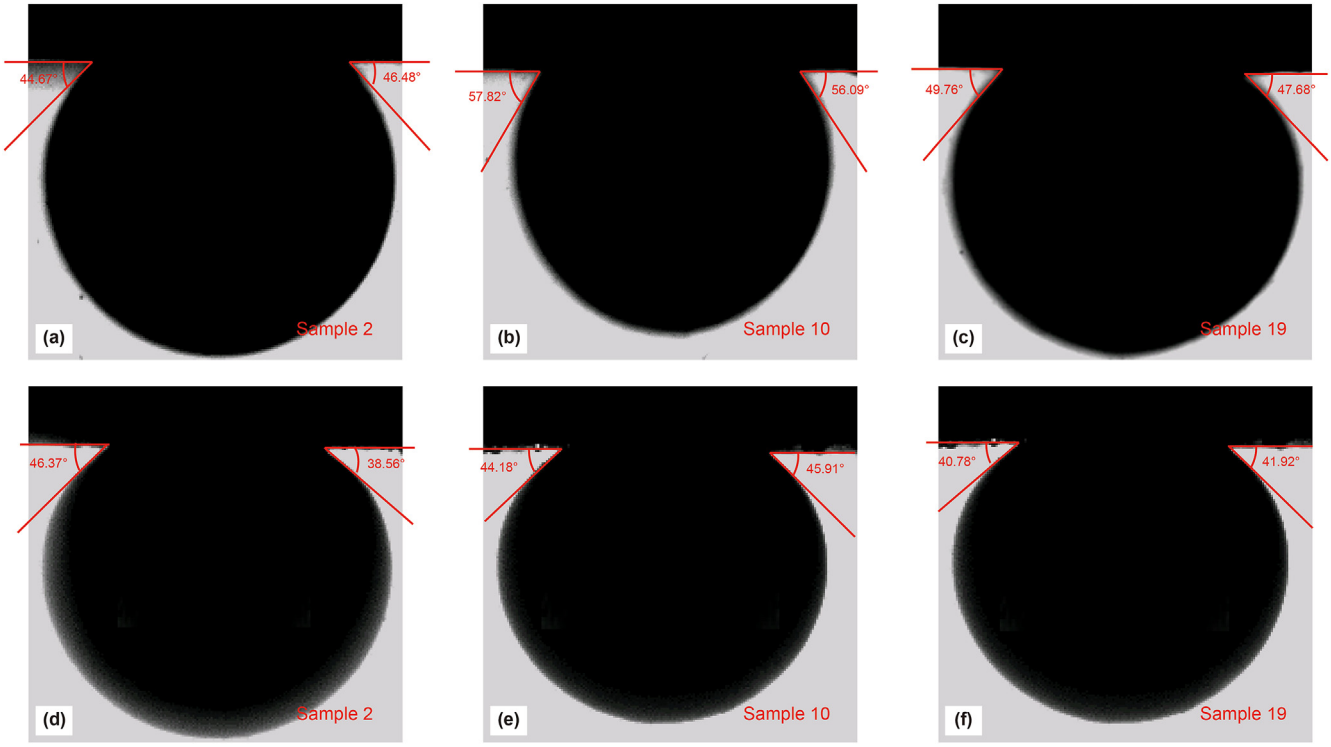

Fig. 7. Measurement of the contact angle between oil drop and core slice in different imbibition fluids. (**a**, **b**, **c)** Contact angles in formation water; (**d**, **e**, **f)** Contact angles in surfactant solution.

Table 7
Summary of imbibition results.

Influencing factor	Core No.	Porosity, %	Permeability, mD	Saturation	Imbibition fluid	Fracture	Recovery, %
Contrast group	1	11.398	0.041	0.839	Distilled water	Non-fracture	18.4
	20	12.081	0.195	0.931	Formation water	Non-fracture	17.7
Fracture	5	12.110	27.209	0.988	Formation water	Single fracture	25.3
	16	7.930	0.136	0.958	Formation water	Cross fracture	21.4
	11	9.020	15.478	1.213	Distilled water	Cross fracture	26.7
Permeability and porosity	8	2.973	0.004	0.918	0.15% SDBS	Non-fracture	23.4
	2	8.933	0.018	0.895	0.15% SDBS	Non-fracture	22.4
	4	11.450	0.036	0.800	0.15% SDBS	Non-fracture	22.3
	10	3.414	0.030	1.015	0.15% SDBS	Non-fracture	8.6
	19	7.228	0.028	0.962	0.15% SDBS	Non-fracture	32.3
	13	11.918	0.033	0.901	0.15% SDBS	Non-fracture	31.4
Surfactant	3	7.441	0.018	0.781	0.05% SDBS	Non-fracture	22.1
	14	7.544	0.013	0.827	0.20% SDBS	Non-fracture	29.4
	19	7.228	0.028	0.962	0.15% SDBS	Non-fracture	32.3

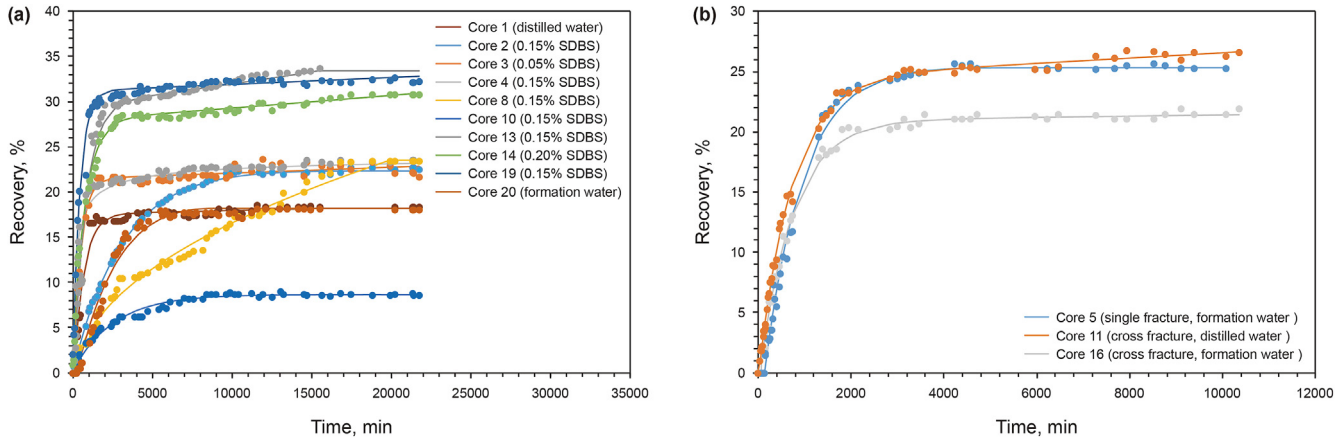

Fig. 8. Curves of tight sandstone imbibition recovery with imbibition time. (**a**) Unfractured core; (**b**) Fractured core.

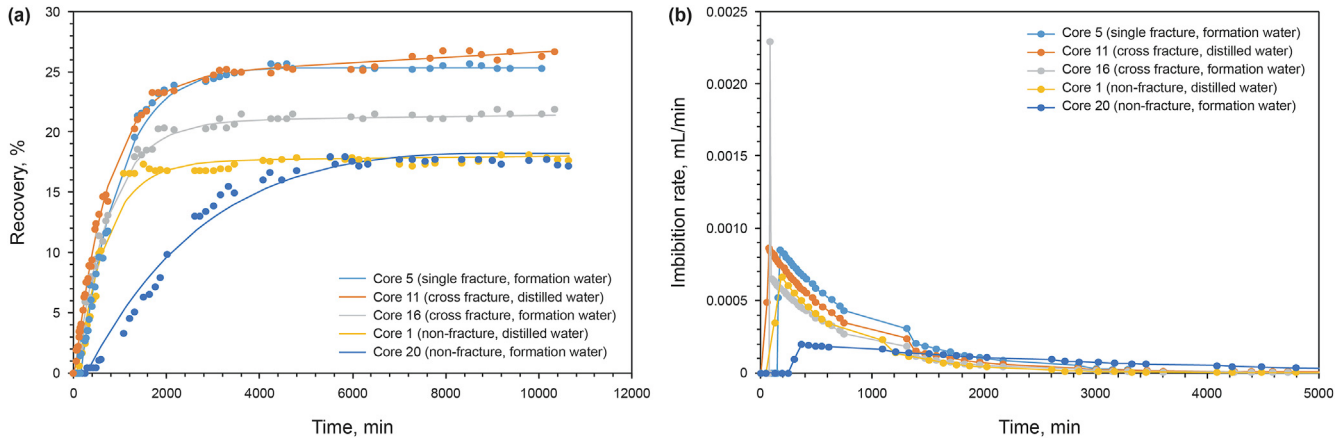

Fig. 9. Imbibition recovery (**a**) and imbibition rate (**b**) of fractured tight sandstones and control tight sandstones.

imbibition rate of the other cores began to decrease, they still do not produce oil. Core 8 has a permeability of 0.004 mD and a porosity of 2.973%. Core 10 has a permeability of 0.030 mD and a porosity of 3.414%. Although the permeability difference between the two cores is about 8 times, their porosity is similar, much lower than other cores. Therefore, we believe that the porosity may make the poor pore throat connectivity and lower seepage capacity. This makes the core imbibition rate slower and the time the oil starts to be produced later than other cores.

5.3. Effect of surfactant on imbibition

Cores 1, 2, 14, 19, and 20 are tested with different imbibition fluids. The recovery and imbibition rate of each core is shown in Fig. 12. Comparing the recovery of each core, it can be found that adding surfactant can improve the recovery of the core and the maximum increase is about 10% (Core 19). Adding surfactant, the contact angle between oil drop and core changes little, but the oil–water interfacial tension changes obviously. With the increase in surfactant mass concentration, the interfacial tension between SDBS and simulated oil decreases. Therefore, we discussed the effect of interfacial tension on imbibition. It can be seen that the core imbibition recovery of 0.05%, 0.15%, and 0.2% SDBS is 22.1% (Core 3), 32.3% (Core 19), and 29.4% (Core 14), respectively. When the oil–water interface tension is too low, the core imbibition recovery begins to decline. Liu (2019) also described this phenomenon. When using cationic surfactant solution as the imbibition liquid, the oil–water interfacial tension is very low, and the imbibition cannot be performed. Therefore, we believe that reducing oil–water interfacial tension to improve imbibition recovery has a certain scope of application. In a certain range, the imbibition recovery increases with the increase in surfactant mass concentration.

Adding surfactant can not only improve the core imbibition recovery but also improve the core imbibition rate in the initial stage of imbibition. The initial imbibition rate increases with the increase in surfactant concentration. As shown in Fig. 13b, the imbibition rate of Core 14 with 0.20% SDBS is the largest in the initial stage of imbibition, followed by Core 19 with 0.15% SDBS, and Core 3 with 0.05% SDBS is the smallest. But similarly, the faster the imbibition rate in the initial stage of imbibition, the faster the imbibition rate decreases in the middle and late stages of imbibition.

During the experiment, the size and distribution of oil droplets on the core surface were observed, as shown in Fig. 13. With the addition of surfactant, the distribution of oil droplets on the core surface is significantly reduced, which may be a reason for the improvement of core imbibition rate and oil recovery. At the same time, it can be seen that the oil droplets, which are produced under the action of capillary force, are mainly distributed on the core surface texture.

In addition, it can be found from Fig. 12 that the imbibition recovery and imbibition rate of Core 1 are higher than Core 20. The

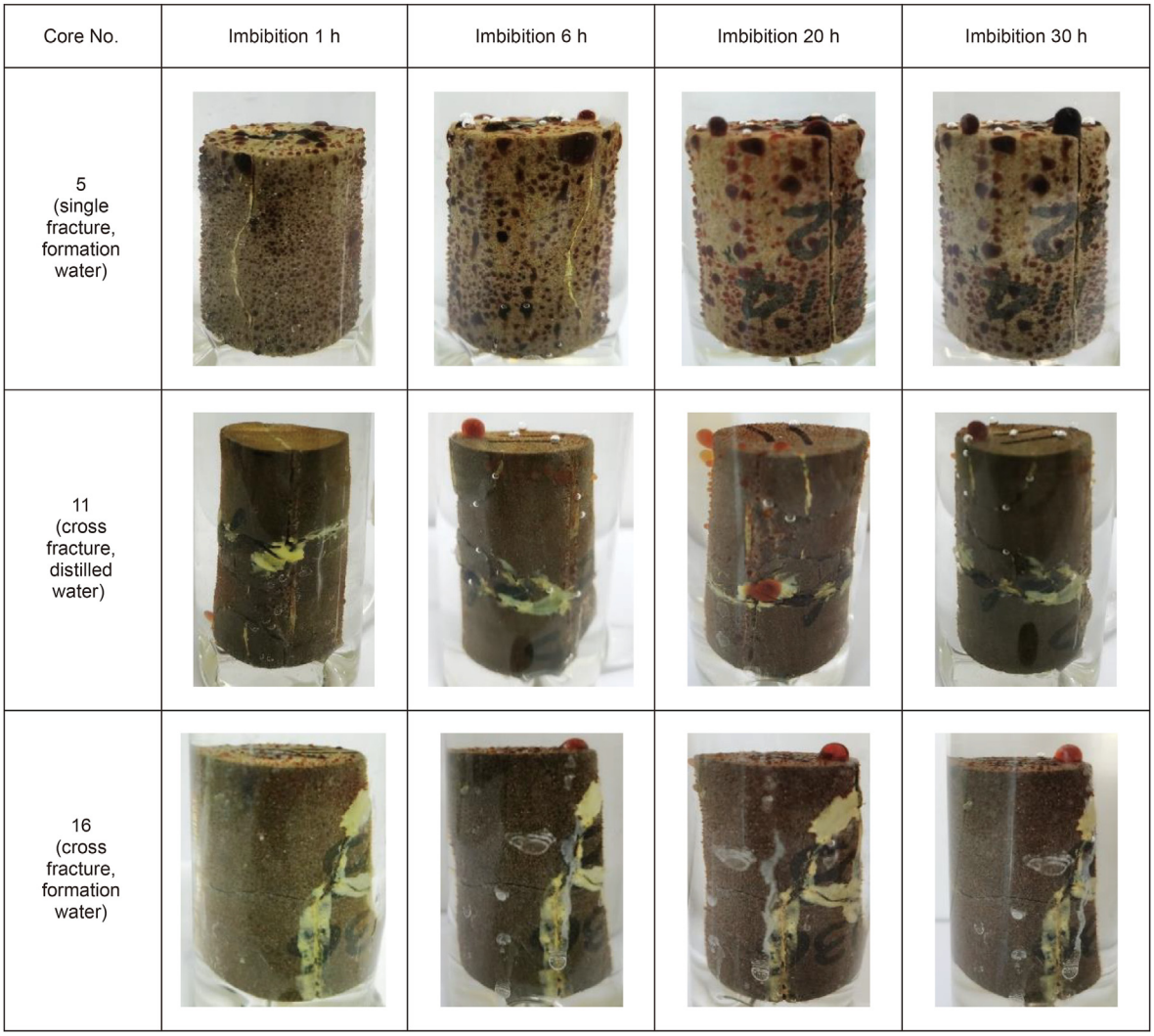

Fig. 10. Variation of oil droplets adsorbed on the surface of three cores. The first row is Core 5, the second row is Core 11, and the third row is Core 16.

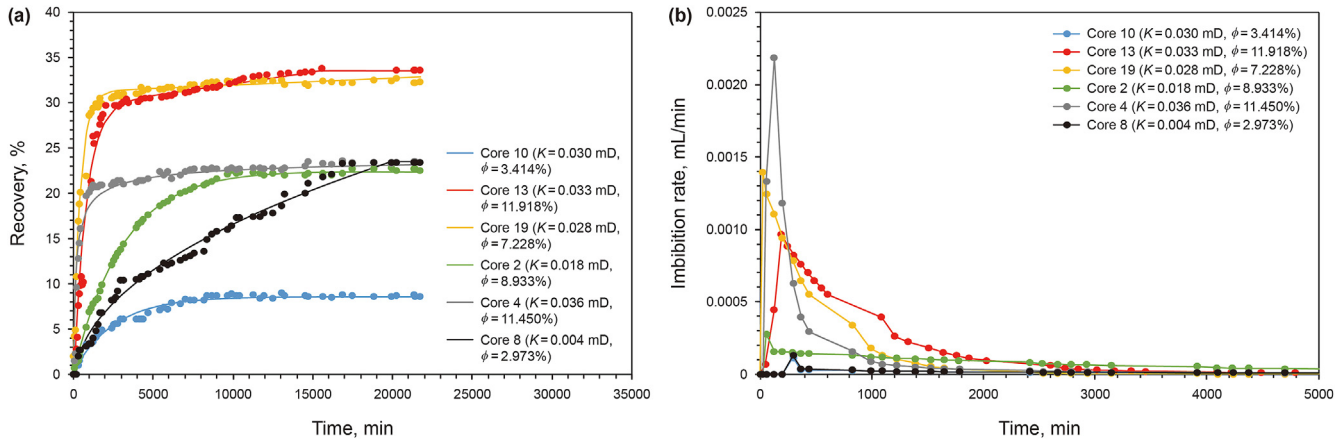

Fig. 11. Imbibition recovery (**a**) and imbibition rate (**b**) of cores with different porosity and permeability.

imbibition fluid of Core 1 is distilled water, and the imbibition fluid of Core 20 is formation water. The difference in salinity between the two imbibition fluids may be the main reason for the large difference in the imbibition rate of the two cores. This phenomenon has also been observed in the imbibition experiment of tight sandstone with fractures. When distilled water as the imbibition fluid, the imbibition recovery is significantly higher than the formation water as the imbibition fluid, as shown in Table 7. Studies have shown that

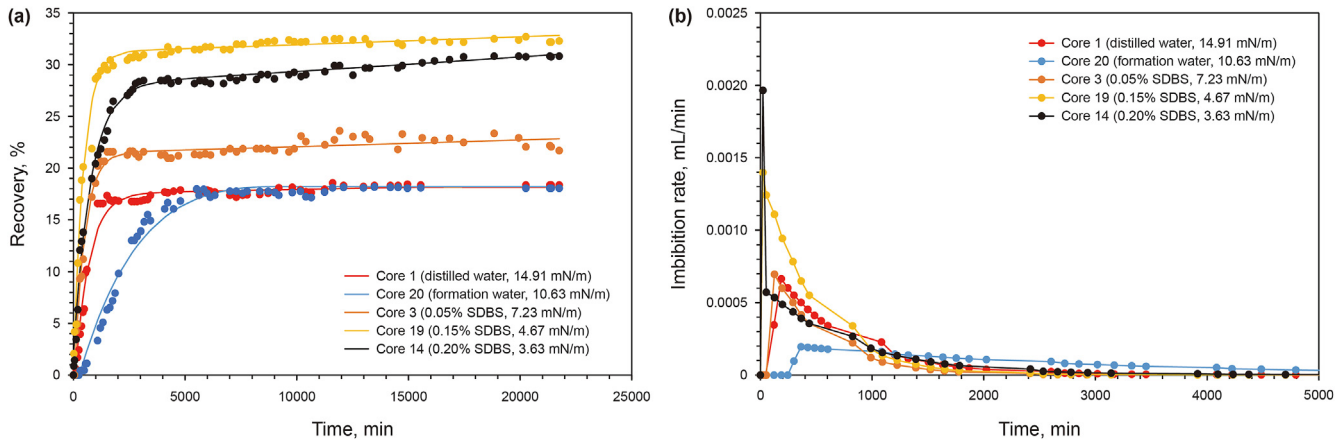

Fig. 12. Imbibition recovery (**a**) and imbibition rate (**b**) of cores in different imbibition fluids.

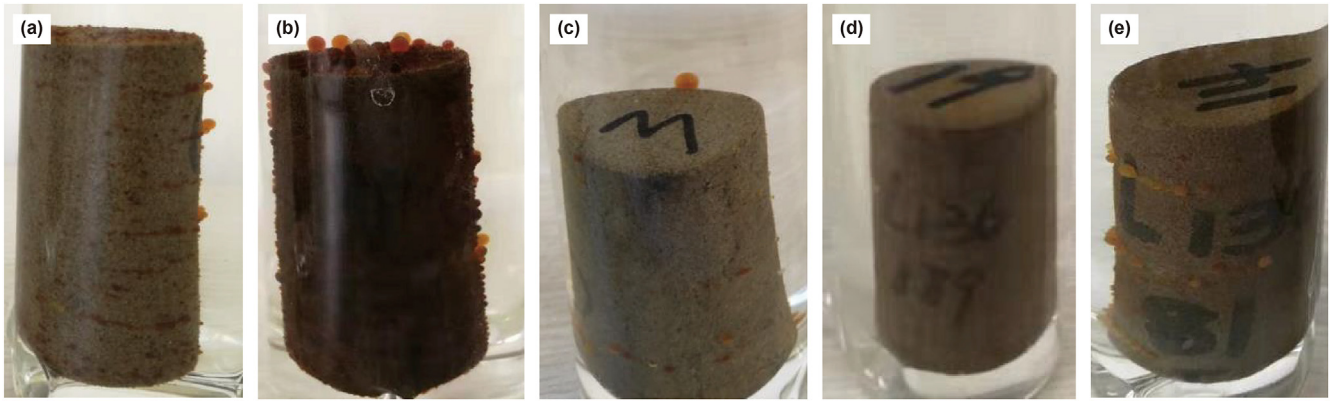

Fig. 13. Size and distribution of oil droplets on the core surface during imbibition. (**a**) Core 1 in distilled water; (**b**) Core 20 in formation water; (**c**) Core 3 in 0.05% SDBS; (**d**) Core 19 in 0.15% SDBS; (**e**) Core 14 in 0.20% SDBS.

the imbibition fluid with low salinity is conducive to the adsorption of water to the core surface, accelerates the shedding of oil droplets on the core surface, and improves the imbibition recovery (Yang et al., 2016b; Zhu et al., 2022). Comparing the adsorption of oil droplets on the surfaces of the two cores, it can be found that Core 20 has larger and more oil droplets adsorbed on the core surface.

6. Conclusions

In this study, combined with HPMI and NMR experiments, the pore-throat structures of the Chang 7 tight sandstone were described. Through physical fracturing experiments, interfacial tension and wettability tests, the influence of fractures, core porosity and permeability, and surfactants on imbibition are studied, and the following conclusions are drawn:

(1) The pores of tight sandstone from the Chang 7 formation in the Erdos Basin are dominated by micro-nano pores, with pores radius concentrated at 0.01–1 μm. Compared with HPMI, NMR can additionally measure pores of 1–10 nm in the cores, to accurately describe the distribution of nano-pores in the tight sandstone.

(2) Fractures can improve imbibition recovery in tight cores with a maximum increase of about 10%. The existence of fractures provides channels for fluid seepage in the core and reduces the adsorption of oil droplets on the core surface. In the early stage of imbibition, with the increase in the number of fractures, the number of oil droplets adsorbed on the core surface decreases, and the imbibition rate increases exponentially.

(3) The core porosity and permeability have a great influence on the core imbibition rate. The greater the porosity and permeability of the cores, the higher the imbibition rate in the early stage of imbibition and the earlier the oil is displaced out. At the same time, oil recovery increases with better pore connectivity.

(4) Surfactant can improve the oil imbibition recovery about 15% by enhancing the water wettability of the core surface, reducing the interfacial tension and reducing the adsorption of oil droplets on the core surface. Besides, the imbibition fluid with low salinity is conducive to the adsorption of water to the core surface, accelerates the shedding of oil droplets, and improves the imbibition rate and oil recovery.

Acknowledgement

This work was supported by the National Natural Science Foundation of China (No. 51874320).

References

Alvarez, J.O., Saputra, I.W.R., Schechter, D.S., 2018. The impact of surfactant imbibition and adsorption for improving oil recovery in the Wolfcamp and Eagle Ford Reservoirs. SPE J. 23, 2103–2118. https://doi.org/10.2118/187176-PA.
Cai, J., Li, C., Song, K., et al., 2020. The influence of salinity and mineral components

on spontaneous imbibition in tight sandstone. Fuel 269, 117087. https://doi.org/10.1016/j.fuel.2020.117087.
Cheng, Z., Ning, Z., Yu, X., et al., 2019. New insights into spontaneous imbibition in tight oil sandstones with NMR. J. Petrol. Sci. Eng. 179, 455–464. https://doi.org/10.1016/j.petrol.2019.04.084.
Dai, C., Cheng, R., Sun, X., et al., 2019. Oil migration in nanometer to micrometer sized pores of tight oil sandstone during dynamic surfactant imbibition with online NMR. Fuel 245, 544–553. https://doi.org/10.1016/j.fuel.2019.01.021.
Deng, L., King, M.J., 2019. Theoretical investigation of the transition from spontaneous to forced imbibition. SPE J. 24, 215–229. https://doi.org/10.2118/190309-PA.
Gao, L., Yang, Z., Shi, Y., 2018. Experimental study on spontaneous imbibition characteristics of tight rocks. Adv. Geo-Energy Res. 2 (3), 292–304. https://doi.org/10.26804/ager.2018.03.07.
Guo, J., Li, M., Chen, C., et al., 2020. Experimental investigation of spontaneous imbibition in tight sandstone reservoirs. J. Petrol. Sci. Eng. 193, 107395. https://doi.org/10.1016/j.petrol.2020.107395.
Johnstone, B., 2007. Bakklen black gold. Leader-Poster 2007-12-10 (6).
Lai, J., Wang, G., Cao, J., et al., 2018. Investigation of pore structure and petrophysical property in tight sandstones. Mar. Petrol. Geol. 91, 179–189. https://doi.org/10.1016/j.marpetgeo.2017.12.024.
Li, A., Ren, X., Wang, G., et al., 2015. Characterization of pore structure of low permeability reservoirs using a nuclear magnetic resonance method. J. China Univ. Petroleum 39 (6), 92–98. https://doi.org/10.3969/j.issn.1673-5005.2015.06.012.
Li, Y., Lu, S., Xia, D., et al., 2022. Development characteristics and main controlling factors of natural fractures in shale series of the seventh member of the Yanchang Formation, southern Ordos Basin. Chinese J. Geol. 57 (1), 73–87. https://doi.org/10.12017/dzkx.2022.004.
Li, C., Singh, H., Cai, J., 2019. Spontaneous imbibition in shale: a review of recent advances. Capillarity 2 (2), 175–182. https://doi.org/10.26804/capi.2019.02.01.
Liu, J., 2018. Sedimentary System and Reservoir Rharacteristics of Chang 7 Member of the Triassic Yangchang Formation in Ordos Basin. Ph.D. Dissertation. Northwest University, Xi'An, p. 168.
Liu, Z., 2019. The Study on Seepage Regularity and Imbibition Enhanced Oil Recovery of Tight Sandstone Reservoir. China university of petroleum (beijing), Beijing, p. 87.
Liu, J., Sheng, J.J., 2020. Investigation of countercurrent imbibition in oil-wet tight cores using NMR technology. SPE J. 25 (5), 2601–2614. https://doi.org/10.2118/201099-PA.
Liu, D., Ren, D., Du, K., et al., 2021. Impacts of mineral composition and pore structure on spontaneous imbibition in tight sandstone. J. Petrol. Sci. Eng. 201, 108397. https://doi.org/10.1016/j.petrol.2021.108397.
Mason, G., Morrow, N.R., 2013. Developments in spontaneous imbibition and possibilities for future work. J. Petrol. Sci. Eng. 110, 268–293. https://doi.org/10.1016/j.petrol.2013.08.018.
Meng, Q., Liu, H., Wang, J., 2017. A critical review on fundamental mechanisms of spontaneous imbibition and the impact of boundary condition, fluid viscosity and wettability. Adv. Geo-Energy Res. 1 (1), 1–17. https://doi.org/10.26804/ager.2017.01.01.
Ning, X., Ewing, R., Hu, Q., et al., 2022. A new model for simulating the imbibition of a wetting-phase fluid in a matrix-fracture dual connectivity system. Geofluids 1–18. https://doi.org/10.1155/2022/7408123.
Saputra, I.W.R., Park, K.H., Zhang, F., et al., 2019. Surfactant-assisted spontaneous imbibition to improve oil recovery on the eagle ford and wolfcamp shale oil reservoir: laboratory to field analysis. Energy & Fuels 33 (8), 6904–6920. https://doi.org/10.1021/acs.energyfuels.9b00183.
Schembre, J.M., Kovscek, A.R., 2001. Direct measurement of dynamic relative permeability from CT monitored spontaneous imbibition experiments. In: SPE Annual Technical Conference and Exhibition. https://doi.org/10.2118/71484-MS.
Shi, J., Xue, Z., Durucan, S., 2011. Supercritical CO_2 core flooding and imbibition in Berea sandstone — CT imaging and numerical simulation. Energy Proc. 4, 5001–5008. https://doi.org/10.1016/j.egypro.2011.02.471.
Song, W., 2021. Research on the Characteristics of Chang 7 Reservoir in the West of Xin'anbian, Ordos Basin. Xi'An Shiyou University, Xi'An, p. 67.
Volokitin, Y., Looyestijn, W.J., Slijkerman, W.F.J., et al., 2001. A practical approach to obtain primary drainage capillary pressure curves from NMR core and log data. Petrophysics 42 (4), 334–343. SPWLA-2001-v42n4a3.
Wang, F., Zhao, J., 2021a. Mathematical model of liquid spontaneous imbibition into gas-saturated porous media with dynamic contact angle and gravity. Chem. Eng. Sci. 229, 116139. https://doi.org/10.1016/j.ces.2020.116139.
Wang, F., Zhao, J., 2021b. Mathematical modeling of gravity and buoyancy effect on low interfacial tension spontaneous imbibition in tight oil reservoirs. AIChE J. 67 (9), 1–15. https://doi.org/10.1002/aic.17332.
Wang, Y., Zhu, Y., Chen, S., et al., 2014. Characteristics of the nanoscale pore structure in northwestern hunan shale gas reservoirs using field emission scanning electron microscopy, high-pressure mercury intrusion, and gas adsorption. Energy & Fuels 28 (2), 945–955. https://doi.org/10.1021/ef402159e.
Wang, J., Liu, H., Xia, J., et al., 2017. Mechanism simulation of oil displacement by imbibition in fractured reservoirs. Petroleum Exploration Dev. Online 44 (5), 805–814. https://doi.org/10.1016/S1876-3804(17)30091-5.
Wang, F., Yang, K., Cai, J., 2018. Fractal characterization of tight oil reservoir pore structure using nuclear magnetic resonance and mercury intrusion porosimetry. Fractals 26 (2), 1840017. https://doi.org/10.1142/S0218348X18400170.
Wang, F., Yang, K., You, J., et al., 2019. Analysis of pore size distribution and fractal dimension in tight sandstone with mercury intrusion porosimetry. Results Phys. 13, 102283. https://doi.org/10.1016/j.rinp.2019.102283.
Xie, K., Lu, X., Pan, H., et al., 2018. Analysis of dynamic imbibition effect of surfactant in microcracks of reservoir at high temperature and low permeability. SPE Prod. Oper. 33, 596–606. https://doi.org/10.2118/189970-PA.
Xu, D., Bai, B., Wu, H., et al., 2019. Mechanisms of imbibition enhanced oil recovery in low permeability reservoirs: effect of IFT reduction and wettability alteration. Fuel 244, 110–119. https://doi.org/10.1016/j.fuel.2019.01.118.
Yang, J., Dong, Z., Dong, M., et al., 2016. Wettability alteration during low-salinity waterflooding and the relevance of divalent ions in this process. Energy & Fuels 30 (1), 72–79. https://doi.org/10.1021/acs.energyfuels.5b01847.
Yang, Z., Liu, X., Li, H., et al., 2019. Analysis on the influencing factors of imbibition and the effect evaluation of imbibition in tight reservoirs. Petrol. Explor. Dev. 46 (4), 779–785. https://doi.org/10.1016/S1876-3804(19)60235-1.
Yu, F., Gao, Z., Zhu, W., et al., 2021. Experiments on imbibition mechanisms of fractured reservoirs by microfluidic chips. Petrol. Explor. Dev. 48 (5), 1162–1172. https://doi.org/10.1016/S1876-3804(21)60099-X.
Zhang, F., Adel, I.A., Park, K.H., et al., 2018. Enhanced oil recovery in unconventional liquid reservoir using a combination of CO_2 huff-n-puff and surfactant-assisted spontaneous imbibition. SPE Annual Technical Conference and Exhibition. https://doi.org/10.2118/191502-MS.
Zhang, F., Jiang, Z., Sun, W., et al., 2019. A multiscale comprehensive study on pore structure of tight sandstone reservoir realized by nuclear magnetic resonance, high pressure mercury injection and constant-rate mercury injection penetration test. Mar. Petrol. Geol. 109, 208–222. https://doi.org/10.1016/j.marpetgeo.2019.06.019.
Zhang, T., Li, Z., Adenutsi, C.D., et al., 2022. Quantitative investigation of nanofluid imbibition in tight oil reservoirs based on NMR technique. Petrol. Sci. https://doi.org/10.1016/j.petsci.2022.04.013.
Zhou, Z., Abass, H., Li, X., et al., 2016. Experimental investigation of the effect of imbibition on shale permeability during hydraulic fracturing. J. Nat. Gas Sci. Eng. 29, 413–430. https://doi.org/10.1016/j.jngse.2016.01.023.
Zhu, D., Li, B., Li, H., et al., 2022. Effects of low-salinity water on the interface characteristics and imbibition process. J. Petrol. Sci. Eng. 208, 109564. https://doi.org/10.1016/j.petrol.2021.109564.